5-16-2023

Revisiting the definition of field capacity as a functional parameter in a layered agronomic soil profile beneath irrigated maize

Paolo Nasta
University of Naples Federico II

Trenton E. Franz
University of Nebraska-Lincoln, trenton.franz@unl.edu

Justin P. Gibson
University of Nebraska - Lincoln, Lindsay Corporation

Nunzio Romano
University of Naples Federico II

Agricultural Water Management 284 (2023) 108368

Contents lists available at ScienceDirect

Agricultural Water Management

journal homepage: www.elsevier.com/locate/agwat

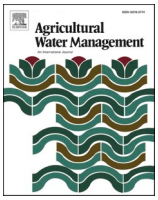

Revisiting the definition of field capacity as a functional parameter in a layered agronomic soil profile beneath irrigated maize

Paolo Nasta [a,*], Trenton E. Franz [b], Justin P. Gibson [b,c], Nunzio Romano [a]

[a] Department of Agricultural Sciences, Division of Agricultural, Forest and Biosystems Engineering, University of Naples Federico II, Napoli, Italy
[b] School of Natural Resources, University of Nebraska-Lincoln, Lincoln, NE 68583, USA
[c] Lindsay Corporation, Omaha, NE 68022, USA

ARTICLE INFO

Handling Editor - J.E. Fernández

Keywords:
Hydrus-1D
On-farm observations
Fertilizer application
Irrigation scheduling
Nitrate leachate
Functional analysis

ABSTRACT

The soil water content at the condition of field capacity (θ_{FC}) is a key parameter in irrigation scheduling and has been suggested to be determined by running a synthetic drainage experiment until the flux rate (q) at the bottom of the soil profile achieves a predefined negligible value (q_{FC}). We question the impact of q_{FC} on the assessment of field capacity. Moreover, calculating θ_{FC} as the integral mean of the water content profile when q is equal to q_{FC} is strictly valid only for uniform soil profiles. By contrast, this practice is ambiguous and biased for stratified soil profiles due to the soil water content discontinuity at the layer interfaces. In this study, the concept of field capacity was revisited and adapted to practical agronomic heuristics. By resorting to the assessment of root-zone water storage capacity (W), we envision field capacity as a functional hydraulic parameter derived from synthetic irrigation scheduling scenarios to minimize drought stress, drainage, and nitrate leachate below the root zone. A functional analysis was carried out on a 135-cm-thick layered soil profile beneath maize in eastern Nebraska. On-farm irrigation scheduling applications and agricultural practices were recorded for 20 years (2001–2020) at a daily time step. Hydrus-1D was calibrated and validated with direct measurements of the soil water retention curve and soil water content data, respectively, in each soil layer. A set of functional field capacity values was derived from 24 irrigation scheduling scenarios, and the optimal water storage capacity at field capacity (W_{FC}) was approximately 50 cm (corresponding to about 80% saturation in the soil profile). An average irrigation amount of 217.5 mm distributed over 21 events was obtained by using optimal irrigation scheduling, which was initiated when the matric pressure head took on a value of −700 cm and the irrigation rate was set at 1.0 cm d^{-1}. This irrigation practice ensured water storage at approximately the same level (ideally at W_{FC}) by sustaining only evapotranspiration fluxes in the uppermost portion of the root zone and by limiting excessive drainage. This protocol can be transferred to other agricultural fields.

1. Introduction

The active rooting zone of a soil profile acts, from a functional viewpoint, as a reservoir that stores incoming water from precipitation or irrigation events and makes it available for crop use over longer periods of water shortage (Romano and Santini, 2002). Therefore, soil provides a critical interplay between crop and atmospheric demand since soil water storage supplies potential root water uptake (RWU), which is reduced under water stress conditions. In agricultural fields, drought stress is mitigated by irrigation applications to keep RWU at its potential level during the crop growing season. From an operational viewpoint, the main challenge is to set the irrigation schedule and the optimal water amount to improve the design of irrigation-based water management strategies.

A widely-used global indicator for governing irrigation scheduling is the root zone soil water storage capacity available for plant use, or simply, plant available water capacity (PAWC), representing the maximum amount of soil water that can be stored in a soil profile to sustain optimal crop growth and yield. A pragmatic but very simplistic way to determine PAWC is to compute the difference between the water storage capacity at field capacity (W_{FC}) and the permanent wilting point (W_{WP}). Commonly, PAWC is expressed as the difference between the soil water content values at field capacity (θ_{FC}) and permanent wilting point (θ_{WP}), multiplied by the thickness of the root zone (z_r), i.e., PAWC= (θ_{FC}

* Corresponding author.
E-mail address: paolo.nasta@unina.it (P. Nasta).

https://doi.org/10.1016/j.agwat.2023.108368
Received 28 December 2022; Received in revised form 9 May 2023; Accepted 11 May 2023
Available online 16 May 2023

$-\theta_{WP})\times z_r$ (Allen et al., 1998).

When the profile-average soil water content in the rooting zone is less than the wilting point θ_{WP}, then it is commonly assumed that the plant wilts permanently. Although the condition of permanent wilting depends not merely on soil type but especially on plant species (Thomasson, 1995; Garg et al., 2020; Wiecheteck et al., 2020; Torres et al., 2021), a common value for θ_{WP} is the soil water content at the matric pressure of − 1.5 MPa (i.e., a matric head of −15,296 cm of water), based on data from sunflowers used as a reference plant species (Taylor and Ashcroft, 1972).

Field capacity is defined as "the volumetric water content remaining in a soil profile two or three days after having been completely wetted with water and after free drainage beyond the root zone has become negligible" (Veihmeyer and Hendrickson, 1949; Soil Science Society of America, 2008). The field drainage experiment is considered a benchmark method for determining θ_{FC}, which is certainly not exempt from criticism and appears a bit vague (Romano and Santini, 2002; Assouline and Or, 2014; de Jong van Lier and Wendroth, 2016). The tacit assumption is that the soil profile is uniform, initially fully saturated, and subject only to gravity-driven drainage, regardless of the evapotranspiration flux which is assumed as zero. Even though definitions exist for θ_{FC} (or W_{FC}) and θ_{WP} (or W_{WP}), the concepts underlying these variables and their physical meanings are still a matter of debate (Gardner, 1965; Ritchie, 1981; Minasny and McBratney, 2003; Garg et al., 2020; Torres et al., 2021; Turek et al., 2022; Cousin et al., 2022).

In-situ drainage experiments are notoriously cumbersome, although representative of actual field conditions, and the condition of field capacity is attained when the drainage flux at the lower boundary of the soil profile is virtually null (Romano and Santini, 2002). Synthetic drainage experiments can be used when the soil hydraulic properties are known beforehand, and the zero flux and the unit (or, fixed) total hydraulic gradient are set as the upper and lower boundaries of the flow domain, respectively. The θ_{FC} value is computed when the water flux (q) at the bottom of the flow domain is equal to a predefined negligible drainage flux (q_{FC}) (Twarakavi et al., 2009; Assouline and Or, 2014; Reynolds, 2018; Inforsato and de Jong van Lier, 2021). When this condition is attained, the simulated profile-average soil water content is often referred to as the flux-based field capacity (Meyer and Gee, 1999; Nasta and Romano, 2016; Inforsato and de Jong van Lier, 2021).

Choosing a negligible value for q_{FC} is obviously arbitrary, but another limitation arises when the synthetic drainage process is simulated in a layered (heterogeneous) soil profile, which exhibits contrasting vertical textural properties and hydraulic characteristics. When using field capacity as a hydraulic parameter in a bucket-type hydrological model, the soil component of the system is often conceptualized as a uniform (homogeneous) flow domain, and this oversimplification can be considered acceptable if one is interested in computing the lumped water budget (Romano et al., 2011). However, when the concept of PAWC is used to resolve agronomic problems, water dynamics in layered soil profiles should be properly characterized by using a process-oriented hydrological model based on the Richards equation. Under these circumstances, the determination of θ_{FC} as a profile average value is not trivial and is rather weak as well, so it becomes convenient to resort to the assessment of W_{FC} (Nasta and Romano, 2016).

Irrigated agriculture in the High Plains Region of the United States mostly relies on aquifer depletion, especially for maize production, as this crop has high irrigation requirements to achieve maximum yield. The average groundwater levels have declined significantly in the Southern and Central High Plains (i.e., Texas, Oklahoma, and Kansas) and parts of Nebraska (Scanlon et al., 2012). Over the last decades, excessive groundwater depletion has been exacerbated by frequent droughts induced by climate change (Rudnick et al., 2019). Overapplication of nitrogen fertilizers and pesticides is the primary source of groundwater contamination, which further decreases the amount of water available for irrigation. The challenge of irrigated agriculture is to identify a functional value for soil water storage at field capacity by preserving optimal root-zone water contents so to avoid, or at least minimize, the onset of drought stress and excessive drainage (and related contaminant transport towards the aquifer).

In this study, Hydrus-1D was used to simulate water flow and solute transport across a 135-cm-thick agronomic layered soil profile beneath irrigated maize in eastern Nebraska (Šimůnek et al., 2016). In Hydrus-1D, irrigation timing is controlled by a depth-specific user-specified soil pressure head while the irrigation rate is set at prescribed values (Lena et al., 2022). Therefore, the target of this synthetic approach was to perform a sensitivity analysis using different values of the user-specified irrigation rate for maize and soil matric pressure head at a soil depth of 67.5 cm (half of maize's maximum root depth). A total of 24 values for water storage capacity at field capacity (W_{FC}) were estimated, and the optimal value was selected to minimize drought stress, drainage flux (to avoid local water waste), and nitrate leachate (to reduce contaminant vulnerability) below the root zone. The "functional" field capacity has been compared with the conventional synthetic drainage experiment, and the challenge of estimating θ_{FC} is discussed.

2. Experimental work and methods

2.1. Environmental settings and data collection

The study site is in eastern Nebraska, USA, at the University of Nebraska Eastern Nebraska Research and Extension Center (ENREC) near Mead. The field site (US-Ne1, 41.1651 N, −96.4779 W; Fig. 1) is part of the AmeriFlux (Baldocchi et al., 2001) and Long-Term Agricultural Research Networks and has been operating since 2001. The regional climate is of a continental semiarid type with a mean annual precipitation of 784 mm yr^{-1} (according to the AmeriFlux US-Ne1 website). According to the Web Soil Survey data (http://websoilsurvey.nrcs.usda.gov/), the soils at the site are comprised mostly of silt loam and silty clay loam.

Maize (*Zea mays* L.) has been grown at the site under overhead sprinkler irrigation, with the growing season beginning in early May and ending in October (Kalfas et al., 2011). Since 2001, crop management practices (i.e., planting density, cultivars, irrigation, and herbicide and pesticide applications) have been applied according to standard management practices prescribed for production-scale maize systems (Suyker and Verma, 2008). More detailed information about site conditions can be found in Suyker et al. (2004) and Verma et al. (2005). Destructive measurements of the leaf area index (LAI) were carried out approximately every two weeks during the growing season from 2003 to 2020 at specific days of the year (DOY) (Fig. 1c), together with other plant characteristics such as height (cm) and dry above-ground biomass (kg ha^{-1}).

After planting (typically the last week of April to the first week of May), the vegetative stage includes plant emergence and tasseling between the second half of April (DOY = 110) and the first half of July (DOY = 200) while the reproductive stage includes silking, blister, milk, dough, dent, and maturity between the first half of July (DOY = 200) and last week of September (DOY = 275).

The maximum root depth was 135 cm; therefore, we considered a 135-cm-thick soil profile. Soil layers are predominantly classified as Ap, Bt1, Bt2, and BC (Soil Survey Division Staff, 2017). Consequently, four soil layers were established with thicknesses of 0–18 cm, 18–38 cm, 38–75 cm, and 75–135 cm, centered on the sampling depths of 10 cm, 25 cm, 50 cm, and 100 cm, respectively (see Fig. 1b). Soil samples were collected to determine seven soil water retention data pairs, namely the soil water contents at the prescribed pressures of 0 cm, 339.9 cm, 1019.7 cm, 2039.5 cm, 3059.2 cm, 4078.9 cm, and 15,296.1 cm in the pressure plate apparatus (Dane and Hopmans, 2002). The soil samples were dried in the oven for at least 24 h at the standard temperature of 105 °C to measure the oven-dry soil bulk density (ρ_b, in g cm^3). The soil texture was predominantly classified as silty clay. ThetaProbes (Delta-T Devices, Cambridge, UK) were installed at four locations in the study

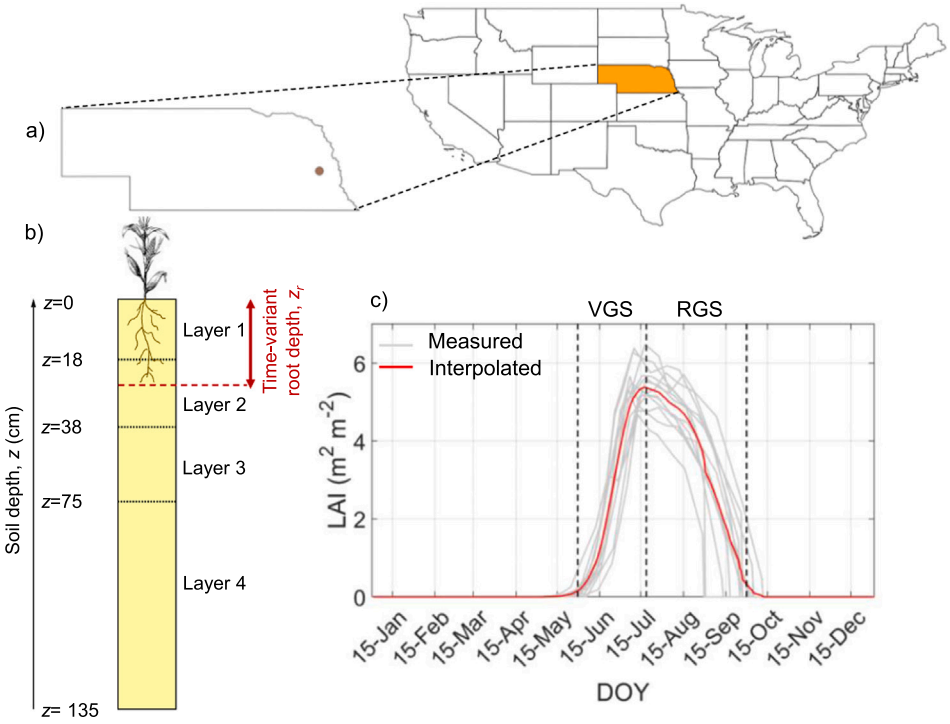

Fig. 1. a) Study site (Mead US-Ne1) location in Nebraska; b) sketch of the 135-cm-thick soil profile with four layers (0–18, 18–38, 38–75, 75–135 cm); root depth (z_r) changes over time during the growing season, and the maximum root depth is 135 cm; c) in-situ measurements of leaf area index (LAI) at the specified day of the year (DOY) (gray line) in each year and daily-mean LAI used for missing years (red line); the vertical dashed lines distinguish between vegetative (VGS) and reproductive (RGS) growth stages for maize.

field with measurement depths of 10, 25, 50, and 100 cm to monitor hourly soil water content in the root zone (Suyker and Verma, 2008).

A flux tower station (Ameriflux and LTAR networks) is located at the same site as the experiment. Hourly/daily values of rainfall (R), minimum, mean, and maximum air temperatures, air relative humidity, wind speed, and net solar radiation are available from 1 January 2001–31 December 2020 (a total of 7305 days corresponding to a 20-year long time series). Daily values of grass-reference potential evapotranspiration (ET_0) were calculated using the physically-based method of Penman-Monteith (Allen et al., 1998).

Assuming a uniform land cover of maize (*Zea mays* L.), crop-specific potential evapotranspiration (ET_c) under standard conditions and without water limitations was calculated by multiplying ET_0 by the specific crop (maize) coefficient, K_c (i.e., $ET_c = ET_0 \times K_c$). The LAI was used to partition ET_c into potential evaporation (E_p) and potential transpiration (T_p) using the following equation:

$$E_P = ET_c e^{-0.463LAI} \quad (1)$$

Potential transpiration, T_p (corresponding to potential root water uptake), was obtained by subtracting potential evaporation (Eq. (1)) from ET_c. The crop coefficient (K_c ranging between 0.20 and 1.06), and the root depth (z_r ranging between 0 cm and 135 cm) were time-variable and were modeled according to the protocol given in Nasta and Gates (2013) and Nasta et al. (2021).

Rainfall interception (I_R) was calculated using the following formula:

$$I_R = aLAI\left(1 - \frac{1}{1 + bP/aLAI}\right) \quad (2)$$

where a (cm d^{-1}) was assumed equal to 0.025 cm d^{-1} and b= 1-$e^{-0.463LAI}$. Interception was subtracted from R to obtain net rainfall (R_{net}). Descriptive statistics of annual mean sums of the aforementioned weather components are reported in Table 2.

In eastern Nebraska, the 100-day-long irrigation season ranges from mid-June (mid-vegetative growth stage) to mid-September (end of reproductive growth stage). Producers usually start irrigating when soil water storage is at the minimum allowable balance in the active root zone (i.e., at the lowest tolerated water storage before the stress begins), which is assumed to be 50% of field capacity, and when no significant rainfall (greater than about 12.7 mm) is expected in the following two-three days. The irrigation amount is given by the difference between water storage at field capacity and the minimum allowable balance over the active root zone and is further subjected to the mechanical system (i.e., well capacity, pumping-curve, field size, and nozzle package). Producers supplied irrigation totals with a mean value of 290 mm to mitigate crop stress.

Fertilizer nutrient requirements for maize are based on expected yield and soil nutrient availability. Nitrogen (N) was mostly applied as urea, $(NH_2)_2CO$, and ammonia, NH_3. Heterotrophic bacteria hydrolyze urea to form ammonium (NH_4^+), which is sequentially nitrified by autotrophic bacteria to nitrite (NO_2^-) and nitrate (NO_3^-). The following three solute species are considered in this study: $(NH_2)_2CO \rightarrow NH_4^+ \rightarrow NO_3^-$. Given the recorded fertilizer applications, we assumed an annual average fertilization amount and timing of 195 kg N ha^{-1} applied on April 1.

2.2. Simulation of water flow and solute transport in Hydrus-1D

Water flow was simulated by numerically solving the Richards equation (Richards, 1931) through the one-dimensional layered soil profile:

$$\frac{\partial \theta}{\partial t} = \frac{\partial}{\partial z}\left[K(\psi)\left(\frac{\partial \psi}{\partial z} + 1\right)\right] - \xi(z, \psi, T_p) \quad (3)$$

where t is time, expressed in units of days (d), ψ is the matric pressure head (cm), z (cm) is the vertical axis (positive upward from the soil surface), θ (cm^3 cm^{-3}) is the volumetric soil water content, and ξ (z, ψ, T_p) is the sink term (d^{-1}) describing the actual plant RWU rate function depending on z, ψ, and potential transpiration (T_p). The flow domain consisted of a heterogeneous (four soil layers) 135-cm-thick soil profile, discretized in 200 nodes with a denser discretization near the soil surface. Hydrus-1D numerically solves the partial-differential equation (Eq. (3)) by using a finite element scheme for spatial discretization and a finite difference scheme for time discretization. The soil water retention, $\theta(\psi)$, and hydraulic conductivity, $K(S_e)$, functions (the so-called soil

hydraulic properties) in each soil layer are described by van Genuchten's equations (van Genuchten, 1980):

$$\theta(\psi) = \theta_r + \frac{\theta_s - \theta_r}{[1 + (|\alpha\psi|^n)]^m} \tag{4}$$

$$K(S_e) = K_s S_e^{\tau}\left[1 - \left(1 - S_e^{1/m}\right)^m\right]^2 \tag{5}$$

where θ_s ($cm^3\ cm^{-3}$) and θ_r ($cm^3\ cm^{-3}$) are the saturated and residual volumetric soil water contents, α (cm^{-1}), n (-) and $m = 1–1/n$ (Mualem restriction) are empirical curve-fitting shape parameters, K_s ($cm\ d^{-1}$) is the saturated hydraulic conductivity, and τ (-) is a tortuosity parameter that is assumed to be $\tau = 0.5$ (Mualem, 1976). The degree of saturation, S_e, varies between 0 (when $\theta = \theta_r$) and 1 (when $\theta = \theta_s$).

Hydrus-1D considers the fate and transport of multiple solutes subjected to first-order degradation reactions. Urea, $(NH_2)_2CO$, degrades to ammonium, NH_4^+, which is subsequently transformed into nitrate, NO_3^-, by the process of nitrification. NO_3^- is then subject to denitrification. The partial differential equations governing the one-dimensional transport of N involved in sequential first-order decay chain reactions during transient water flow in a variably saturated rigid porous medium are taken as:

$$\frac{\partial \theta C_1}{\partial t} = \frac{\partial}{\partial z}\left(\theta D_1^w \frac{\partial C_1}{\partial z}\right) - \frac{\partial q C_1}{\partial z} - \mu'_{w,1}\theta C_1 \tag{6}$$

$$\frac{\partial \theta C_2}{\partial t} + \frac{\partial \rho_b S_2}{\partial t} + \frac{\partial a_v g_2}{\partial t} = \frac{\partial}{\partial z}\left(\theta D_2^w \frac{\partial C_2}{\partial z}\right) + \frac{\partial}{\partial z}\left(a_v D_2^g \frac{\partial g_2}{\partial z}\right) - \frac{\partial q C_2}{\partial z} - \mu'_{w,2}\theta C_2 + \mu'_{w,1}\theta C_1 - r_{a,2} \tag{7}$$

$$\frac{\partial \theta C_3}{\partial t} = \frac{\partial}{\partial z}\left(\theta D_3^w \frac{\partial C_3}{\partial z}\right) - \frac{\partial q C_3}{\partial z} - \mu_{w,3}\theta C_3 + \mu'_{w,2}\theta C_2 - r_{a,3} \tag{8}$$

where C is the solute concentration in the liquid phase ($mg\ L^{-1}$), S is the solute concentration in the solid phase ($mg\ g^{-1}$), g is the solute concentration in the gas phase ($mg\ L^{-1}$), θ is the volumetric water content ($cm^3\ cm^{-3}$), a_v is the air content ($cm^3\ cm^{-3}$), q is the volumetric flux density ($cm\ d^{-1}$), μ_w is the first-order rate constant for the solute in the liquid phase (d^{-1}), μ'_w is the first-order rate constant providing the connection between individual nitrogen species in the liquid phase (d^{-1}), r_a is the root nutrient uptake term ($mg\ L^{-1}\ d^{-1}$), D^w is the dispersion coefficient ($cm^2\ d^{-1}$) for the liquid phase, and D^g is the diffusion coefficient ($cm^2\ d^{-1}$) for the gas phase. The subscripts 1, 2, and 3 represent $(NH_2)_2CO$, NH_4^+, and NO_3^-, respectively.

The dispersion coefficient in the liquid phase, D^w, is given as:

$$D^w = D_L\frac{|q|}{\theta} + D_w\tau_w \tag{9}$$

where D_w is the molecular diffusion coefficient in free water ($cm^2\ d^{-1}$), τ_w is a unitless tortuosity factor in the liquid phase, $|q|$ is the absolute value of the Darcian fluid flux density ($cm\ d^{-1}$), and D_L is the longitudinal dispersivity (cm).

2.3. Model parameterization

In a preliminary step, the parameters (θ_r, θ_s, α, n, and K_s) controlling water flow in Hydrus-1D need to be assessed. The simulated water balance requires validation using soil water content values monitored at different soil depths along the profile.

The lower boundary condition is set to free drainage (downward water flux at the bottom of the soil profile, q) as the mean annual depth to water is about 10 m and has minimal impact on the top few meters of soil (https://snr.unl.edu/data/water/groundwater/realtime/default.aspx). The upper boundary condition depends on the atmospheric fluxes occurring at the soil surface (R_{net} and E_p). When the superficial matric pressure head is less than a default threshold value, then the flux boundary condition at the soil surface automatically switches to a constant pressure head boundary condition, resulting in a reduction of potential evaporation (E_p) into actual evaporation (E_a). A proportion of net rainfall is turned into runoff when the superficial matric pressure head exceeds the maximum soil surface matric head value, representing the nominal depth of surface water ponding allowable before runoff generation. Initial conditions were set by interpolating the measured soil water content values in the soil profile on January 1st, 2001.

Plant potential transpiration, T_p, occurs through the roots, which are linearly distributed along the soil profile, varying from a maximum at the soil surface to a minimum at the time-variant maximum rooting depth. T_p is reduced by water stress to actual transpiration (T_a). The actual RWU rate corresponding to T_a, i.e., the sink term (ξ) in Eq. (3), is modeled using the method proposed by Feddes et al. (1978). Maize T_p is reduced between $\psi = -325$ cm (if $T_p > 0.5\ cm\ d^{-1}$) or $\psi = -600$ cm (if $T_p < 0.1\ cm\ d^{-1}$) and the wilting point that corresponds to $\psi_{wp} = -8000$ cm (Wesseling et al., 1991). Unlimited passive uptakes of both NH_4^+ and NO_3^- were allowed in the root solute uptake model by specifying the maximum allowed uptake concentration exceeding NO_3^- concentrations in the root zone. More details are provided in the Hydrus manual (Šimůnek et al., 2006).

Fertilization was given in the form of urea (solute 1), and a total annual amount of 195 kg N ha^{-1} (corresponding to a solute mass per unit area of 1.95 mg cm^{-2}) was applied on the soil surface in a single treatment on April 1st. The solute parameters featured in the urea–ammonium–nitrate fertigation system subject to nitrogen (N) transformation processes were taken from Hanson et al. (2006), as done by other authors (Ramos et al., 2012; Bradshaw et al., 2013; Nasta et al., 2021).

For each soil layer, the soil hydraulic parameters θ_s, α, and n were fitted to the measured soil water retention data pairs (Eq. (4)). To reduce the number of fitting parameters, we assumed $\theta_r = 0\ cm^3\ cm^{-3}$ (Leij et al., 2005). The Levenberg-Marquardt type parameter optimization algorithm embedded in Hydrus-1D was used to estimate the K_s values of each layer by minimizing the difference between simulated and observed soil water content values at the soil depths of 10 cm, 25 cm, 50 cm, and 100 cm during the growing season ($N = 3603$). The comparison between observations and model simulations in the dormant season ($N = 3702$) was ignored in the inverse modeling since information on snow accumulation, snow melting, and soil freezing-defrosting processes was missing. In Hydrus-1D, four observation points were placed at each of these soil depths.

Model performance measures are based on the root mean square error (RMSE) and coefficient of determination (R^2), defined as:

$$RMSE = \sqrt{\frac{1}{n}\sum_i^n (O_i - P_i)^2} \tag{10}$$

$$R^2 = \frac{\sum_i^n (O_i - P_i)^2}{\sum_i^n (O_i - \overline{O})^2} \tag{11}$$

where O, $\overline{O}$, and P are the observed, mean of observed, and predicted values of soil water content at time step i expressed in days (n is the total number of time steps). For an optimum prediction, values should be as low as possible for RMSE and as close as possible to 1 for R^2.

In addition, the performance metric Kling-Gupta efficiency (KGE) is defined as (Gupta et al., 2009):

$$KGE = 1 - \sqrt{(r-1)^2 + (\beta - 1)^2 + (\gamma - 1)^2} \tag{12}$$

where r is Pearson's correlation coefficient, β is the ratio of estimated and observed means, and γ indicates the ratio of estimated and observed coefficients of variation. Optimal predictions are diagnosed by KGE = 1 as well as by $r = 1$, $\beta = 1$, $\gamma = 1$.

2.4. Synthetic approaches to estimate field capacity

Soil water storage at field capacity (W_{FC}) was estimated by using two synthetic approaches (Fig. 2):

1) Synthetic drainage experiment scenarios were used to estimate the flux-based field capacity (W_{FC}) by considering eight negligible drainage fluxes (q_{FC}) (q_{FC} = 0.01, 0.025, 0.05, 0.1, 0.2, 0.3, 0.4, 0.49 cm d^{-1}) proposed in the literature (red box in Fig. 2; Section 2.4.1) (Nachabe, 1998; Romano and Santini, 2002; Twarakavi et al., 2009; de Jong van Lier and Wendroth, 2016; Reynolds, 2018; Turek et al., 2020);
2) Synthetic irrigation scheduling scenarios were used to estimate 24 functional field capacity (W_{FC}) values by considering local on-farm practices (Payero et al., 2008; Rudnick et al., 2016); the W_{FC} value that results in minimum drought stress (or maximum percentage of T_a/T_p), minimum drainage flux (q) and nitrate leaching at the lower boundary (blue box in Fig. 2; Section 2.4.2) was selected as the optimal functional field capacity.

2.4.1. Estimation of flux-based field capacity from drainage experiment scenarios

The synthetic drainage experiment assumes an initially saturated soil profile, one-dimensional vertical gravity-driven flow (no lateral flow), null water flux across the soil surface (evaporation and rainfall set to zero), and no water uptake by roots ($\xi = 0$). Solute transport is neglected in this simulation, and the soil hydraulic parameters (θ_s, α, n, and K_s) in each soil layer were assessed in Section 2.3.

The initial and boundary conditions were the following:

$$\psi(z,t) = 0 \text{ for } 0 \geq z \geq z_r \text{ at } t=0 \tag{13}$$

$$q(z,t) = q_0 = 0 \text{ at } z = 0, \forall\, t \geq 0 \tag{14}$$

$$\frac{\partial H}{\partial z} = 1 \quad \text{at} \quad z = z_r, \quad \forall t \geq 0 \tag{15}$$

where z_{FC} is the depth of the model flow domain corresponding to the bottom of the active root zone ($z_r = -135$ cm), and H is the total hydraulic head ($H = z + \psi$). Conditions (14)–(15) impose: (*i*) zero soil matric head ($\psi = 0$) throughout the soil profile at the beginning of the simulation (i.e., an initially saturated, gravity-draining soil profile); (*ii*) zero water flux at the soil surface ($q_0 = 0$ at $z = 0$) for $t \geq 0$; and (*iii*) free drainage ($\partial H/\partial z = +1$) at the lower boundary ($z = z_r$).

The water storage at field capacity (W_{FC}) in the root zone is defined as (Romano and Santini, 2002):

$$W_{FC} = \sum_{i=1}^{N} \theta_i \Delta z_i \tag{16}$$

where θ_i is soil water content at each *i*-th node and N is the total number of nodes within the selected z_r, Δz_i is nodal spacing, and $\sum_{i=1}^{N} \Delta z_i = |z_r|$. W_{FC} is determined (Eq. (16)) when the flux at the bottom of the root zone (q) reaches a prescribed threshold value, q_{FC} (q_{FC} = 0.01 cm d^{-1}, 0.025 cm d^{-1}, 0.05 cm d^{-1}, 0.1 cm d^{-1}, 0.2 cm d^{-1}, 0.3 cm d^{-1}, 0.4 cm d^{-1}, and 0.49 cm d^{-1}) at drainage time, t_{FC} (Inforsato and de Jong van Lier, 2021; Turek et al., 2022). It is worth noting that, due to the discontinuity of the soil water contents across the interface of the soil layers, the value of θ_{FC} cannot be computed as the integral mean of the water content profile recorded at a certain time.

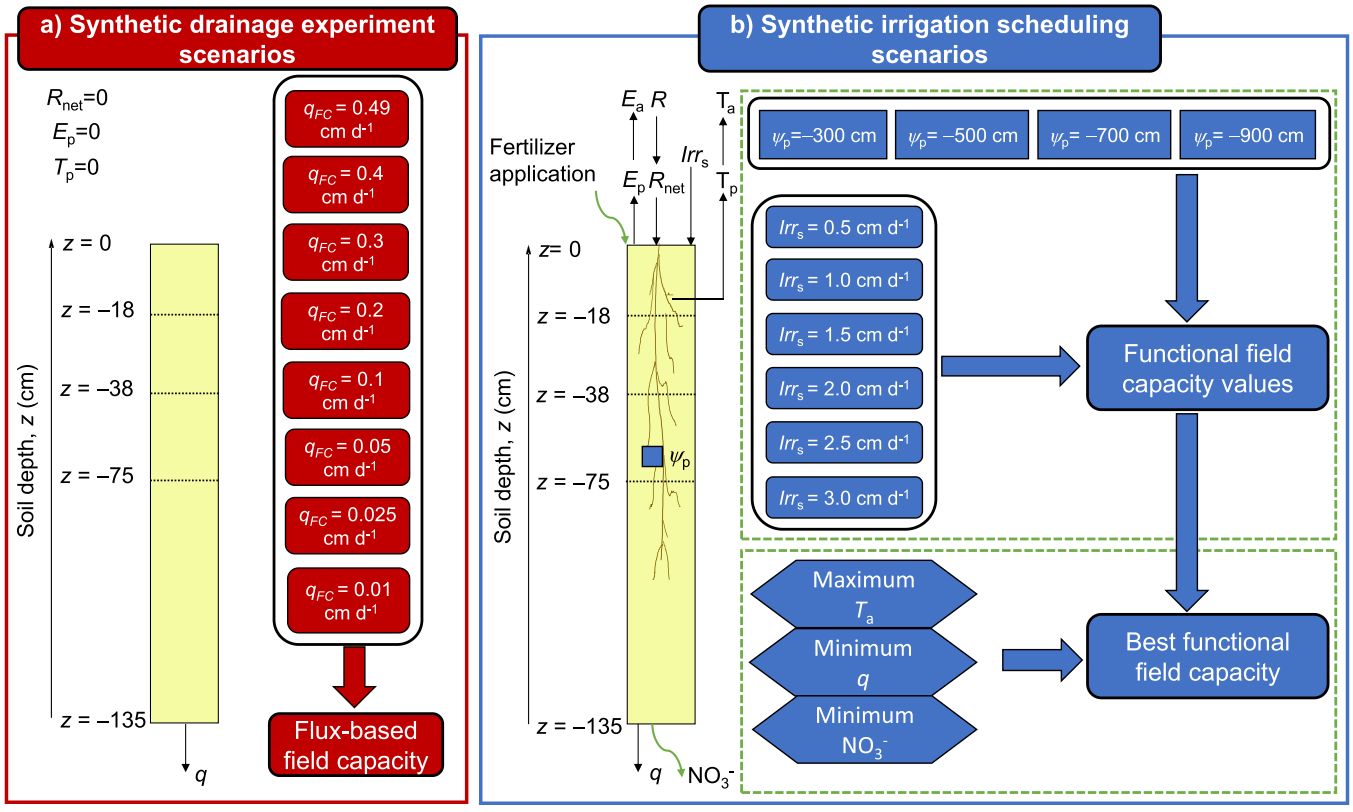

Fig. 2. Schematic overview of the proposed methodology to assess: a) flux-based field capacity with eight synthetic drainage experiment scenarios depending on prescribed negligible fluxes, q_{FC} (red box), and b) functional field capacity with 24 synthetic irrigation scheduling scenarios depending on the combination of four prescribed matric pressure head values, ψ_p, and six user-specified irrigation rates, Irr_s (blue box). These prescribed values originate from site-specific farming practices reported in the field and in the body of literature. R, R_{net}, E_p, T_p, q, E_a, T_a, and NO_3^- indicate gross rainfall, net rainfall, potential evaporation, potential transpiration, drainage flux, actual evaporation, actual transpiration, and nitrate concentration, respectively.

2.4.2. Estimation of a functional field capacity condition from irrigation scheduling scenarios

The initial and boundary conditions are the same as described in Section 2.3. The soil hydraulic parameters (θ_s, α, n, and K_s) of each soil layer were assessed according to the criteria described in Section 2.3. To mitigate excessive crop water stress during the growing season, Hydrus-1D has the option to trigger a user-specified irrigation rate (Irr_s) when a prescribed pressure head (ψ_p) is reached at a given observation node. Irrigation starts after a user-specified lag period at a user-specified irrigation rate. The duration of irrigation is also specified.

The irrigation scheduling scenarios were obtained by running Hydrus-1D repeatedly by changing:

i) the prescribed matric pressure head values at which irrigation is initiated ($\psi_p = -300$ cm, $\psi_p = -500$ cm, $\psi_p = -700$ cm, $\psi_p = -900$ cm) at an observation node located at the soil depth of 67.5 cm, i.e., half of the maximum root depth (blue square in the soil profile in Fig. 2),
ii) the specified irrigation rates ($Irr_s = 0.5$ cm d^{-1}, $Irr_s = 1.0$ cm d^{-1}, $Irr_s = 1.5$ cm d^{-1}, $Irr_s = 2.0$ cm d^{-1}, $Irr_s = 2.5$ cm d^{-1}, $Irr_s = 3.0$ cm d^{-1}).

For simplicity, both the lag period and duration of irrigation were set to 1 day. The functional field capacity as the water storage (W_{FC}) in the active root zone (Eq. (16)) was determined at the end of the synthetic irrigation event (after 1 day, as we set both duration and lag equal to 1 day). The water and solute balance components were stored for each model simulation.

3. Results

3.1. Model parameterization and water and nitrate balance in the irrigated plot

Whereas the Hydrus-1D model uses the basic units of length in cm, for convenience, the water balance components are presented here as units of length in mm. The optimized soil water retention parameters for each soil layer are reported in Table 1, whereas Fig. 3 shows the comparison between observed and simulated soil water content values at the four soil depths of $z = 10$ cm, $z = 25$ cm, $z = 50$ cm, and $z = 100$ cm. The shape of the water retention curve is mostly influenced by the values of n and α featured in Eq. (4). The soil water retention function of the deepest soil layers ($z = 75$–135 cm) has the lowest values of n and α, and is characterized by a smooth decay in soil water content with increasing pressure head values. The optimized values of θ_s and K_s show a decreasing pattern towards the deeper layers, and this behavior is mainly induced by soil compaction (Turkeltaub et al., 2020). The prediction performance (RMSE and R^2) metrics reported in Table 1 are fair despite the fact that we suspect the model was ill-informed by the sensors located at two soil depths. The removal of observed soil water content values in the last five years ($N = 1098$) at soil depths of 10 cm and 100 cm for suspicious malfunctioning (especially the deepest layer, see Fig. 3e) enhanced the RMSE and R^2 values (Table 1) and proved to be satisfactory if compared to previous studies in agricultural fields (Wollschläger et al., 2009; Wöhling and Vrugt, 2011; Ket et al., 2018; Sao et al., 2021). The best KGE was obtained in the deepest layer, where soil water content was kept constantly near fully saturated conditions (Fig. 3e). In contrast, the seasonal variability of the observed soil water content was difficult to match in the first three soil layers (Fig. 3b-d), and this is depicted by relatively lower KGE values (Table 1). This was corroborated by a scrutiny of the three KGE scores (r, β, and γ, not reported in Table 1). The correlation coefficients passed the 0.05 significance test in all layers and ranged between 0.435 in the second layer and 0.473 in the fourth layer. The β values were close to unity for all layers, indicating unbiased predictions. While on the one hand, r and β values were similar in all layers, on the other hand, γ values controlled KGE along soil depth, with the farthest ($\gamma = 1.492$) and the closest ($\gamma = 0.984$) from optimum ($\gamma = 1$) for the second and fourth layer, respectively.

The variability of simulated water content values (standard deviations of 0.0609 cm^3 cm^{-3}, 0.0618 cm^3 cm^{-3}, 0.0415 cm^3 cm^{-3}, and 0.0097 cm^3 cm^{-3} at soil depths of 10 cm, 25 cm, 50 cm, and 100 cm, respectively) was higher than the one of corresponding observations in the first three soil depths (standard deviations of 0.0542 cm^3 cm^{-3}, 0.0489 cm^3 cm^{-3}, 0.0383 cm^3 cm^{-3}, and 0.0113 cm^3 cm^{-3} at soil depths of 10 cm, 25 cm, 50 cm, and 100 cm, respectively).

The impact of tillage operations on soil porosity was ignored, but we are aware that it might influence the soil hydraulic properties of the uppermost soil layer (Schlüter et al., 2018; Hu et al., 2018; Fu et al., 2021; Talukder et al., 2022).

The mean water balance in the irrigation seasons (corresponding to the 100-day-long period ranging from mid-June to mid-September) in 2001–2020 is reported in Table 2. The inter-annual variability of water balance components was mainly controlled by rainfall variability, which ranged from 50.4 mm to 248.6 mm with a mean value of 146.7 mm. The amount of water supplied by rainfall in the irrigation season was not sufficient to meet the average crop-specific potential evapotranspiration demand (ET_c =236.8 mm).

As the total water supplied by precipitation and irrigation exceeded the crop water requirement during the irrigation season, ET_a represented 92% of ET_c when using simulations with irrigation. Average annual drainage represented about 20% of precipitation and irrigation by inducing on average 0.376 mg cm^{-2} (corresponding to 37.6 kg N ha^{-1} or 19.2% of applied fertilizer) nitrate leachate. The mean annual drought stress, namely the difference between potential (T_p) and actual (T_a) transpiration, was 19.1 mm and 36.0 mm with or without irrigation scheduling, respectively. Reductions in drainage (−8.5 mm) and nitrate leaching (−0.075 mg cm^{-2} or −7.5 kg N ha^{-1}) are reported when removing the irrigation events (Table 2).

3.2. Estimation of flux-based field capacity from drainage simulation scenarios

The decrease in water storage over time derived from the simulation of the draining process across the layered soil profile is presented in Fig. 4a. Theoretically, water storage and the corresponding drainage flux, q, at the bottom of the active root zone (Fig. 4b), decrease for very

Table 1
Optimized soil hydraulic parameters (saturated soil water content, θ_s, water retention shape parameters, α and n, and saturated hydraulic conductivity, K_s) in the four soil layers and corresponding performance metrics quantified through root mean square error (RMSE), coefficient of determination (R^2), and Kling-Gupta efficiency (KGE) when comparing observed and simulated soil water content values (the number in each soil layer is indicated by N) at soil depths of 10 cm, 25 cm, 50 cm, and 100 cm.

Profile Interval cm	θ_s cm^3 cm^{-3}	α cm^{-1}	n -	K_s cm d^{-1}	N -	RMSE cm^3 cm^{-3}	R^2 -	KGE -
0–18	0.502	0.00321	1.452	50.2	2505	0.0660	0.228	0.329
18–38	0.502	0.00321	1.452	10.3	3603	0.0671	0.190	0.251
38–75	0.463	0.00551	1.255	30.6	3603	0.0465	0.228	0.393
75–135	0.456	0.00059	1.135	4.50	2505	0.0124	0.167	0.473

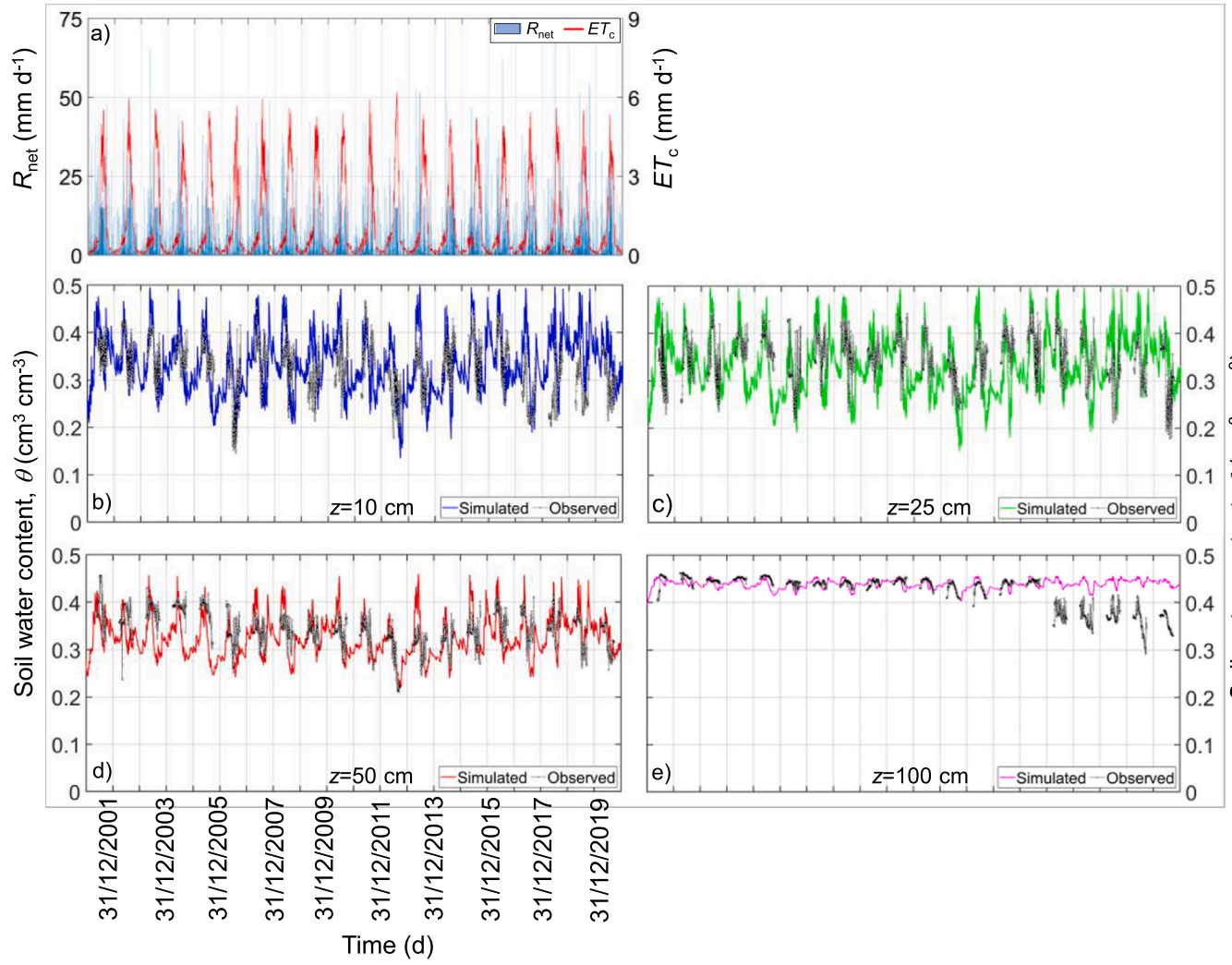

Fig. 3. a) Daily net rainfall, R_{net} (blue bars), and potential evapotranspiration, ET_c (red line); observed (black circles) soil water content (θ) values are compared to simulated ones at soil depths of b) $z = 10$ cm (blue line), c) $z = 25$ cm (green line), d) $z = 50$ cm (red line), and e) $z = 100$ cm (magenta line).

Table 2
Mean, standard deviation (*SD*), minimum (*Min*), and maximum (*Max*) of annual net rainfall (R_{net}), potential evaporation (E_p), potential transpiration (T_p), drainage (q), actual evaporation (E_a), and actual transpiration (T_a) for the growing seasons (July, August, and September) of 2001–2020.

	Input weather data			Irrigation scheduling				Without irrigation scheduling			
	R_{net} mm	E_p mm	T_p mm	q mm	E_a mm	T_a mm	NO_3^- mg cm^{-2}	q mm	E_a mm	T_a mm	NO_3^- mg cm^{-2}
Mean	146.7	26.8	210.0	87.0	26.8	190.9	0.376	38.6	26.8	174.0	0.101
SD	59.0	9.5	14.1	16.5	9.5	15.8	0.083	17.5	9.5	22.0	0.062
Min	50.4	16.6	183.1	83.2	16.6	149.5	4.30E-04	68.1	16.6	116.8	6.89E-07
Max	248.6	63.0	238.7	18.7	63.0	217.5	0.352	12.8	63.0	197.8	0.234

long periods. We report the field capacity (W_{FC}) at which q is equal to a predefined negligible flux, q_{FC} (Table 3).

We report t_{FC}-values between 4 d and 391 d and corresponding W_{FC}-values between 60.4 cm and 39.2 cm at the maximum ($q_{FC} = 0.49$ cm d^{-1}) and minimum ($q_{FC} = 0.01$ cm d^{-1}) q_{FC}-values, respectively. Only the first prescribed negligible flux provides a drainage time that is consistent with the classical definition given by, i.e., "*the amount of water held in soil after excess water has drained away and the rate of downward movement has materially decreased, which usually takes place within 2–3 days after a rain or irrigation in pervious soils of uniform structure and texture*".

Fig. 5 shows the vertical distribution of soil matric head and soil water content values at the eight drainage times listed in Table 3. Note that, during the evolution of the drainage process, soil matric head profiles are continuous in the entire flow domain, whereas soil water content profiles are discontinuous across the interface of layers characterized by contrasting soil hydraulic properties (Romano et al., 1998). In other words, at a fixed drainage time (t_{FC}), one can compute the profile-averaged matric head, but the discontinuity of water content profiles hinders the calculation of the integral mean for function $\theta(z,t_{FC})$ in the entire flow domain. This drawback raises further vagueness when assessing the soil water content at the condition of field capacity in the case of stratified soil profiles. Nevertheless, due to similar soil hydraulic functions of the first three soil layers (-75 cm $< z < 0$ cm; see the

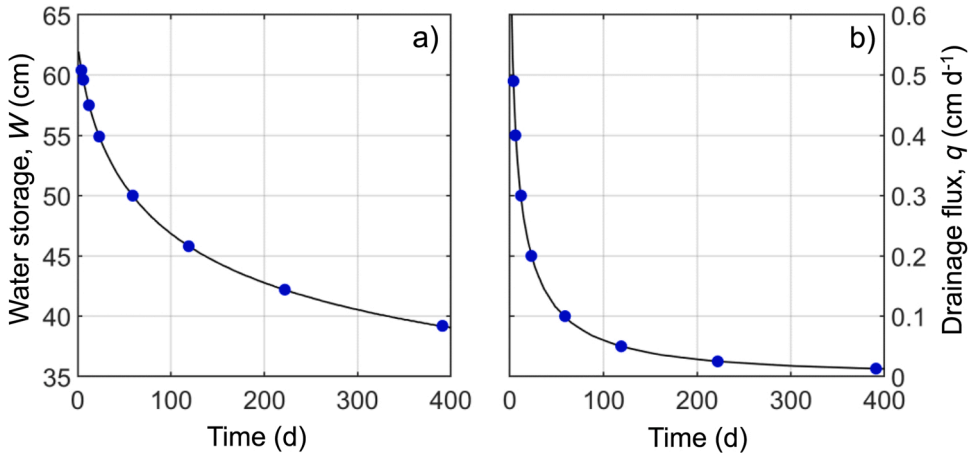

Fig. 4. Results of the simulated drainage process with a) the depletion of soil water storage (W) and b) the decay in drainage flux (q) at the lower boundary over time. The blue circles indicate the drainage time and soil water storage values when q equals eight prescribed negligible drainage fluxes, q_{FC}, given in the literature (q_{FC} = 0.01, 0.025, 0.05, 0.1, 0.2, 0.3, 0.4, 0.49 cm d^{-1}).

Table 3
Drainage time, t_{FC}, and water storage capacity at field capacity, W_{FC}, for eight prescribed negligible fluxes, q_{FC}, reported in the literature.

q_{FC}	t_{FC}	W
cm d^{-1}	d	cm
0.49	4	60.4
0.4	6	59.6
0.3	12	57.5
0.2	23	54.9
0.1	59	50.0
0.05	119	45.8
0.025	222	42.2
0.01	391	39.2

hydraulic parameters in Table 1), Fig. 5b shows that the resulting soil water contents across the soil layer boundaries vary little, and therefore an average θ-value can be assumed to be roughly representative from the soil surface ($z = 0$) to the soil depth of 75 cm, especially for the times around 59 days after the initiation of the simulation (Nasta and Romano, 2016).

3.3. Estimation of functional field capacity from irrigation scheduling scenarios

The results of the 24 synthetic irrigation scheduling scenarios are shown in Fig. 6. We calculated the water and nitrate balance components in the 100-day-long irrigation season: total irrigation amount (*Irr*), number of irrigation events (N), actual transpiration (T_a), drainage (q) and cumulative nitrate flux (NO_3^- flux).

The four prescribed matric pressure heads (ψ_p) are distinguished by different colors in Fig. 6 and control the number of irrigation events (Fig. 6b). Triggering irrigation at a low matric head value (ψ_p = −900 cm, yellow bars) induced the lowest number of irrigation events ($N = 5$) and the lowest amount of total irrigation (*Irr* ranging from 27 mm to 162 mm). In contrast, triggering irrigation at a pressure head (ψ_p = −300 cm, green bars) close to the beginning of drought stress induced the highest number of irrigation events (N ranging from 14 to 30) and the largest amount of irrigation sums (*Irr* ranging from 154 mm to 423 mm). T_a and q were correlated with the total amount of irrigation (Fig. 6a-c-d). Frequent irrigation applications (green bars in Fig. 6a) induced the largest T_a and q sums (green bars in Fig. 6c-d). The water (q) and nitrate leachate fluxes obtained by fixing Irr_s = 0.5 cm d^{-1} and ψ_p = −300 cm were similar to those obtained without irrigation

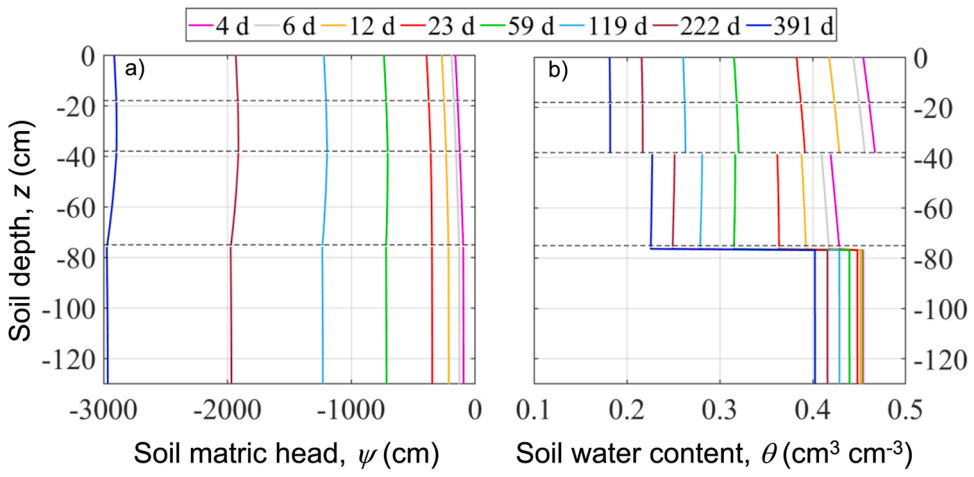

Fig. 5. Time evolution of a) the soil matric head, ψ, and b) soil water content, θ, profiles at the eight drainage times listed in Table 3. The horizontal dashed lines delimit the four soil layers.

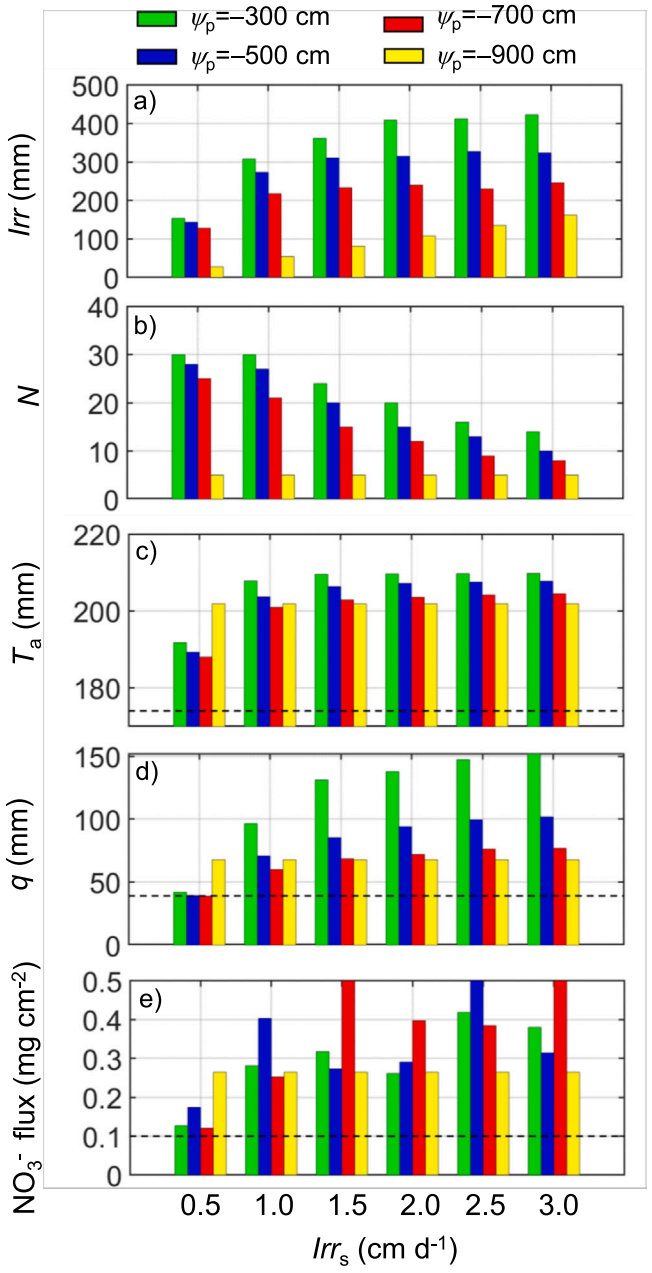

Fig. 6. Irrigation season (from mid-June to mid-September) mean values of a) irrigation amount (*Irr*), b) number of irrigation events (*N*), c) actual transpiration sums (T_a), d) drainage sums (q), e) cumulative nitrate flux (NO_3^- flux) for user-specified irrigation rates (Irr_s) and prescribed matric pressure head values ($\psi_p = -300$ cm, $\psi_p = -500$ cm, $\psi_p = -700$ cm, $\psi_p = -900$ cm, indicated by the green, blue, red, and yellow bars, respectively). Horizontal dashed lines indicate reference values obtained from simulations without irrigation.

scheduling. The irrigation management based on $Irr_s > 0.5$ cm d^{-1} and $\psi_p = -300$ cm prevented the initiation of crop stress but would require many irrigation applications at the cost of obtaining the largest drainage and high nitrate contamination. When irrigation was initiated under sub-optimal water conditions ($\psi_p = -700$ cm and $\psi_p = -900$ cm), simulated T_a and q were lower than those obtained with $\psi_p = -300$ cm. Nevertheless, T_a was quite insensitive to irrigation rates higher than 1.0 cm d^{-1} (Fig. 6c-d). The nitrate leachate was correlated to drainage but also depended on the reaction parameters (transforming urea into ammonium and ammonium into nitrate), root nitrate uptake dynamics, and fertilization timing and amount. Generally, nitrate leachate ranged between 0.121 mg cm^{-2} (or 12.1 kg N ha^{-1}) and 0.611 mg cm^{-2} (or 61.1 kg N ha^{-1}) obtained when $Irr_s = 0.5$ cm d^{-1} and for $\psi_p = -700$ cm and $Irr_s = 2.5$ cm d^{-1} and for $\psi_p = -500$ cm, respectively (Fig. 6e). The range of nitrate leachate presented in Table 2 and Fig. 6e compares well to a similar field measurement-based study in the region, where measured nitrate leaching represented up to 27% of input for continuous maize (Klocke et al., 1999).

Fig. 7 shows the distribution of field capacity (W_{FC}) values by considering all irrigation scheduling scenarios. The mean of all field capacity values was 51.2 cm, whereas the 25th, 50th, and 75th percentiles were 48.1 cm, 51.4 cm, and 54.6 cm, respectively. The median of field capacity values tended to increase with increasing prescribed pressure heads (from 55.3 cm to 47.9 cm for $\psi_p = -300$ cm and $\psi_p = -900$ cm, respectively) and with increasing irrigation rates.

The pillar of "*more irrigation, less drought stress, more drainage, and more nitrate leaching*" was generally valid and the choice of the best irrigation practice depended on the maximum amount of water the producers were willing to supply, on the maximum crop yield (which in turn depends on the relationship with actual RWU), and on the maximum nitrate leachate allowed by local regulations. When nitrate concentration in groundwater is above 10 mg L^{-1}, the maximum contaminant level (MCL) and hazardous health effects become a concern among humans and animals (https://extensionpublications.unl.edu/assets/pdf/g1784.pdf). In light of these conditions, the best irrigation scheduling (*Irr* = 217.5 mm distributed in 21 events per irrigation season) was determined when fixing $\psi_p = -700$ cm and $Irr_s = 1.0$ cm d^{-1}. This synthetic irrigation scenario ensured a rise in T_a from 174.0 mm (Table 2) to 200.9 mm (Fig. 6c), in q from 38.6 mm (Table 2) to 59.9 mm (Fig. 6d), and in nitrate flux from 0.101 mg cm^{-2} (Table 2) to 0.253 mg cm^{-2} (Fig. 6e). The best irrigation scheduling scenario relied on a 217.5 mm irrigation amount by saving 72.5 mm in each season (when compared to the 290 mm supplied by local producers) and obtained T_a representing about 96% of T_p. The simulated drainage (q = 59.9 mm) and nitrate leaching (0.253 mg cm^{-2}) were lower than those (q = 87.0 mm and 0.376 mg cm^{-2}) simulated by using observed agronomic practices (Table 2).

A range of plausible values for the functional root-zone water storage was calculated using the Student's t distribution for a 95% confidence interval, obtaining average values between 49.7 and 50.3 cm (corresponding approximately to 80% of saturation condition).

Fig. 8 shows an illustrative example of the irrigation application in 2002 by fixing $\psi_p = -700$ cm and supplying water at the rate $Irr_s = 1.0$ cm d^{-1}. On day 613 (5 September 2002), ET_a was 0.24 cm d^{-1} and the profile-average matric head $\psi = -741.1$ cm. Therefore, the irrigation event started because ψ_p reached the threshold value of − 700 cm at the soil depth of 67.5 cm. Then, the irrigation application ended on day 614 (6 September 2002), and both soil water content and matric pressure head values increased in the upper layers of the soil profile by sustaining $ET_a = 0.297$ cm d^{-1}. On day 615 (7 September 2002), the uppermost portion of the root zone (i.e., z between 0 cm and 40 cm) rapidly desaturated under dry conditions (as visualized by retreating orange curves in Fig. 8). Nevertheless, the soil water storage capacity ranged between 49.6 cm and 50.2 cm (approximately at the field capacity condition) by limiting drought stress and downward flux.

4. Discussion

Precision agriculture relies on efficient irrigation scheduling to apply water to crops at the right time and in the right amount (Graham et al., 2022; Srinivasan et al., 2022; Kumar et al., 2022). Smart irrigation enables farmers to save water without subjecting crops to moisture deficiency and adverse environmental impacts (Bwambale et al., 2022). The functional field capacity (blue box in Fig. 2b) was derived from the optimal irrigation scheduling scenario by minimizing crop water stress, excessive drainage, and nitrate leaching in an agronomic layered soil profile beneath maize in eastern Nebraska. In this study, we found a mean seasonal irrigation total of 217.5 mm distributed over 21 daily

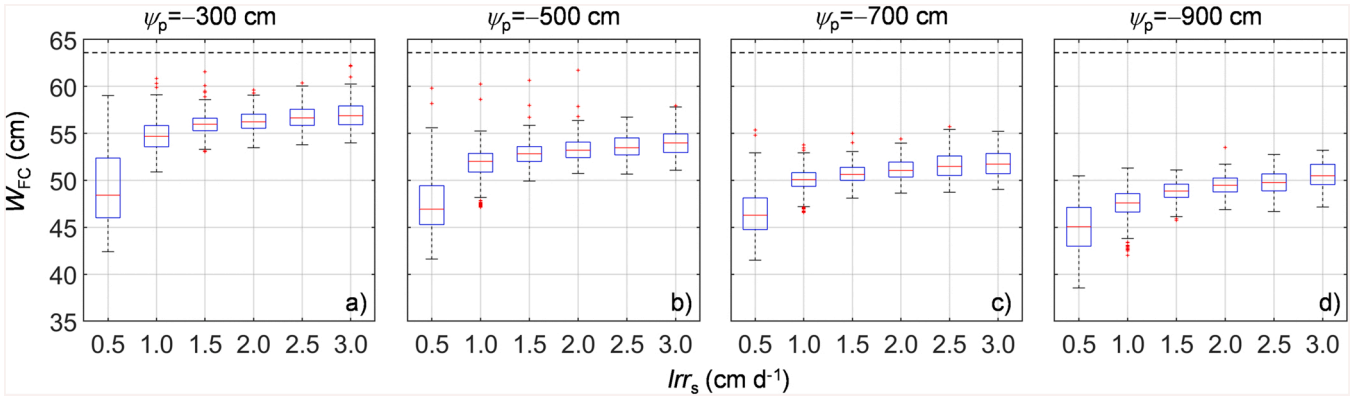

Fig. 7. Box-plots of soil water storage at field capacity (W_{FC}) for different irrigation rates (Irr_s) and four prescribed matric pressure head values for initiating irrigation: a) $\psi_p = -300$ cm, b) $\psi_p = -500$ cm, c) $\psi_p = -700$ cm, d) $\psi_p = -900$ cm. The horizontal dashed line indicates the water storage at saturation ($W_s = 63.6$ cm).

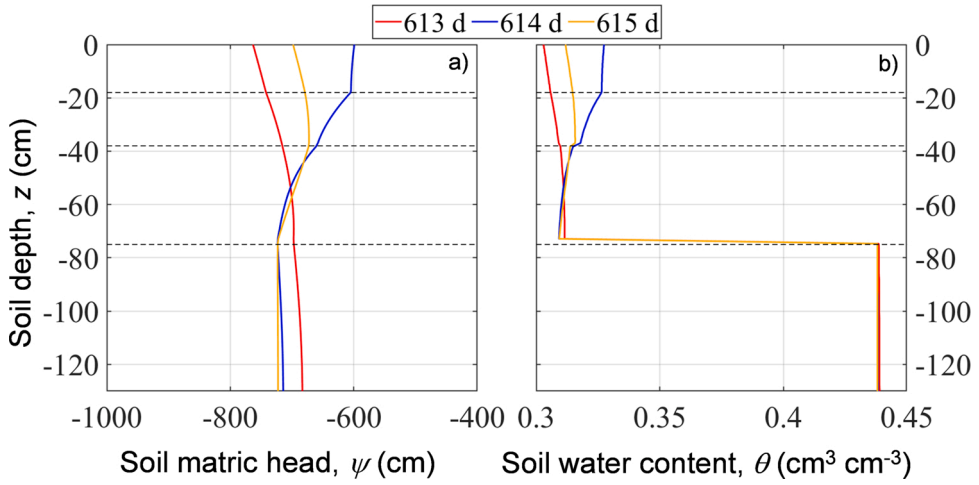

Fig. 8. Time evolution of a) the soil matric head, ψ, and b) soil water content, θ, profiles at days 613, 614, and 615. Irrigation was initiated on day 613 and ended on day 614 when water storage (W_{FC}) at field capacity was recorded. The horizontal dashed lines delimit the four soil layers.

events. On average, simulated irrigation water was supplied every five days at a rate of 1 cm d^{-1}. In Mead, irrigation usually ranges between 230 mm and 350 mm and is applied with a rate of 0.65 cm d^{-1} per 3-day-long period to ensure a full rotation of the pivot due to its speed (Suyker and Verma, 2009; Gibson et al., 2017). Frequent irrigation applications with relatively low rates are beneficial for crop growth but in practice might be affected by evaporation loss from the sprinklers, therefore, future studies should consider the tradeoff between maintenance factors and optimal irrigation scheduling.

Nitrate leaching is controlled by fertilization timing and amount, nitrogen transformations, root nitrate uptake dynamics, and water movement, which, in turn, are influenced by the soil hydraulic properties of each soil layer, atmospheric boundary conditions, and irrigation management (Weitzman et al., 2022). In this study, nitrate leachate (0.252 mg cm^{-2} or 25.2 kg N ha^{-1}) derived from the best irrigation scheduling scenario represents 13% of the fertilizer amount (1.95 mg cm^{-2} or 195 kg N ha^{-1}). High transpiration fluxes favored by irrigation supply during the irrigation season induce root nitrate uptake rates at their maximum level by limiting nitrate migration below the root zone. Samani et al. (2020) found mean annual nitrate leaching of 52 kg N ha^{-1} and 91 kg N ha^{-1} for continuous corn and for corn-soybean rotation at Mead (NE).

We neglected the economic criterion of efficiency because costs and prices are volatile and fluctuate rapidly from year to year, whereas the relationship between drought stress and crop yield needs to be carefully assessed in a follow-up study (Sharma and Irmak, 2020; Zhang et al., 2021a, 2021b). Crop yield was ignored in this study because it would require specific on-farm measurements and a detailed crop growth model (Létourneau et al., 2015; Vogeler et al., 2019; Kelly et al., 2023).

The other model simulation (red box in Fig. 2a) refers to a synthetic drainage experiment enabling the flux-based field capacity to be assessed. The determination of the flux-based field capacity is a non-trivial task and should follow a standard protocol by removing, as much as possible, all vague criteria related to the duration of the synthetic drainage process (Veihmeyer and Hendrickson, 1949; Ritchie, 1981; Wilcox, 1959; Assouline and Or, 2014; Armindo and Wendroth, 2016). A further difficulty arises because real-world soil profiles are layered rather than uniform (Nasta and Romano, 2016).

That said, we pose the following questions: what is the negligible flux rate at which simulated drainage is assumed null? What is the corresponding drainage time?

A first attempt is to take advantage of the information on soil water storage depletion over time. This task can be performed using quantitative or qualitative techniques based on the soil water storage decay over time simulated during the synthetic drainage process. A qualitative and somewhat subjective technique has been illustrated by Zotarelli et al. (2019), who reported a very practical, but rather subjective way of detecting the condition of field capacity in actual agronomic soils as the point of intersection of the two tangents at the curve depicting the water storage depletion: one tangent drawn some hours or a few days

(fast-drainage slope) and the other tangent drawn several days or even several months (slow-drainage slope) after the start of drainage. By applying this empirical approach to the soil water storage depletion curve shown in Fig. 4, it was found that the root-zone water storage capacity at field capacity (W_{FC}) is 53.7 cm, about 25 days after the beginning of the model simulation.

A rough quantitative estimation of the drainage time (t_{FC}) at the condition of field capacity was obtained by using the analytical method developed by Ogata and Richards (1957) and verified by Wilcox (1959). The soil water storage depletion curve of Fig. 4 was interpolated with a power function [$W(t) = 78.7 \times t^{-0.117}$, for t greater than 1 day] whose derivative enabled us to obtain $t_{FC} = 57.2$ d by fixing the negligible drainage flux $dW/dt = q_{FC} = 0.10$ cm d^{-1} as suggested by Meyer and Gee (1999), and hence to obtain W_{FC}= 49.1 cm.

Furthermore, in most cases, smart irrigation systems rely on low-cost capacitance sensors to monitor soil water content at different soil depths across the soil profile. Therefore, a convenient and practical rule to ascertain the condition of field capacity in the soil profile is to refer to the resolution of a sensor that expresses the extent to which the target variable can change to be recorded by the datalogger. New-generation capacitance sensors have a resolution of approximately 0.001 cm^3 cm^{-3} and, accounting for the simulation results, this entails that the soil water storage depletion can no longer be detected at approximately 50 days after the initiation of the synthetic drainage process.

As a conclusive comment on the multiple aspects covered in this discussion section, we point out that the flux-based water storage at field capacity obtained from the synthetic drainage process is quite similar to the functional value of water storage capacity ($W_{FC} = 50$ cm) reported in Table 3 at $q_{FC} = 0.10$ cm d^{-1} and $t_{FC} = 59$ days. Yet, the drainage time at field capacity obtained from the synthetic drainage process should only be considered a fictitious parameter that allows comparing the two simulation scenarios used in this study (see the schematics in Fig. 2), but certainly cannot correspond to the maximum interval allowed between irrigations (i.e., the so-called irrigation frequency) if water is supplied at the rate $Irr_s = 1.0$ cm d^{-1}.

5. Conclusions

Efficient irrigation scheduling optimizes the application of water at the right time and in the right amount. Field capacity represents the threshold storage needed to control the optimal irrigation amount by limiting the negative effects related to underwatering and overwatering. Applying more than the required irrigation water triggers excessive drainage and nitrate leaching. By contrast, supplying inadequate irrigation amounts may lead to crop stress and a reduction in crop yield. In this study, we assessed the functional water storage at field capacity by minimizing crop water stress and potential negative effects on the environment such as excessive drainage and nitrate leaching in a layered soil profile beneath maize in eastern Nebraska. We tested 24 irrigation scheduling scenarios by changing irrigation timing and rate. The lowest drought stress, drainage, and nitrate leachate were obtained by triggering irrigation near optimal conditions ($\psi_p = -300$ cm) for irrigation rates higher than 0.50 cm d^{-1}. By contrast, increasing the irrigation rates and amounts is detrimental in terms of drainage and groundwater contamination without further benefits for root water uptake. Therefore, an optimal compromise was found when fixing $Irr_s = 1.0$ cm d^{-1} and $\psi_p = -700$ cm. The functional water storage field capacity (W_{FC}) derived from this irrigation practice was between 49.70 and 50.30 cm, but this value cannot be directly converted into soil water content at field capacity (θ_{FC}) for the layered soil profile.

The synthetic drainage experiment is used for assessing the flux-based field capacity that is obtained when the drainage flux at the lower boundary of the soil profile is approximately null. The functional analysis carried out in this study is useful to correct the vagueness in the synthetic drainage process when the field capacity concept was adapted to practical agronomic heuristics. This protocol can be transferred to other agricultural fields under different climates, soil, and crop characteristics. Moreover, the implementation of improved irrigation scheduling schemes can help minimize adverse tradeoffs between water quality and water quantity that exist throughout the Midwest USA.

Declaration of Competing Interest

The authors declare that they have no known competing financial interests or personal relationships that could have appeared to influence the work reported in this paper.

Data availability

Data will be made available on request.

Acknowledgments

The authors acknowledge financial assistance from Lindsay Corporation supporting this work. Funding for these AmeriFlux core sites at the Eastern Nebraska Research and Extension Center was provided by the U.S. Department of Energy's Office of Science. This research was a contribution from the Long-Term Agroecosystem Research (LTAR) network. LTAR is supported by the United States Department of Agriculture. T.E.F. acknowledges the financial support of the USDA National Institute of Food and Agriculture, Hatch project #1020768. The Italian partner carried out this study within the "Agritech National Research Center" and received funding from the European Union Next-GenerationEU [Piano Nazionale di Ripresa e Resilienza (PNRR) – Missione 4 Componente 2, Investimento 1.4-D.D. 1032 17/06/2022, CN00000022]. This manuscript reflects only the authors' views and opinions, neither the European Union nor the European Commission can be considered responsible for them.

References

Allen, R., Pereira, L.S., Raes, D., Smith, M., 1998. Crop Evapotranspiration – Guidelines for Computing Crop Water Requirements. FAO Irrigation and Drainage Paper No. 56. Rome, Italy.

Armindo, R.A., Wendroth, O., 2016. Physical soil structure evaluation based on hydraulic energy functions. Soil Sci. Soc. Am. J. 80, 1167–1180.

Assouline, S., Or, D., 2014. The concept of field capacity revisited: defining intrinsic static and dynamic criteria for soil internal drainage dynamics. Water Resour. Res. 50, 4787–4802.

Baldocchi, D., Falge, E., Gu, L., Olson, R., 2001. FLUXNET: a new tool to study the temporal and spatial variability of ecosystem-scale carbon dioxide, water vapor, and energy flux densities. Bull. Am. Meteorol. Soc. 82, 2415–2434.

Bradshaw, J.K., Radcliffe, D.E., Šimůnek, J., Wunsch, A., McCray, J.E., 2013. Nitrogen fate and transport in a conventional onsite wastewater treatment system installed in a clay soil: a nitrogen chain model. Vadose Zone J. 12 (3), 20. https://doi.org/10.2136/vzj2012.0150.

Bwambale, E., Abagale, F.K., Anornu, G.K., 2022. Smart irrigation monitoring and control strategies for improving water use efficiency in precision agriculture: a review. Agric. Water Manag. 260, 107324 https://doi.org/10.1016/j.agwat.2021.107324.

Cousin, I., Buis, S., Lagacherie, P., Doussan, C., Le Bas, C., Guérif, M., 2022. Available water capacity from a multidisciplinary and multiscale viewpoint. A review. Agron. Sustain. Dev. 42, 46. https://doi.org/10.1007/s13593-022-00774-8.

Dane, J.H., Hopmans, J.W., 2002. Water retention and storage. In: Dane, J.H., Topp, G.C. (Eds.), Methods of Soil Analysis. Part 4. SSSA Book Series, No. 5. SSSA, Madison, WI, pp. 671–675.

Feddes, R.A., Kowalik, P.J., Zaradny, H., 1978. Simulation of Field Water Use and Crop Yield. John Wiley & Sons, New York, NY.

Fu, Z., Hu, W., Beare, M., Thomas, S., Carrick, S., Dando, J., Langer, S., Müller, K., Baird, D., Lilburne, L., 2021. Land use effects on soil hydraulic properties and the contribution of soil organic carbon. J. Hydrol. 602, 126741.

Gardner, W.R., 1965. Dynamic aspects of soil-water availability to plants. Annu. Rev. Plant Physiol. 16, 323–342.

Garg, A., Bordoloi, S., Ganesan, S.P., Sekharan, S., Sahoo, S., 2020. A relook into plant wilting: observational evidence based on unsaturated soil–plant-photosynthesis interaction. Sci. Rep. 10, 22064. https://doi.org/10.1038/s41598-020-78893-z.

Gibson, J., Franz, T.E., Wang, T., Gates, J., Grassini, P., Yang, H., Eisenhauer, D., 2017. A case study of field-scale maize irrigation patterns in western Nebraska: implications for water managers and recommendations for hyper-resolution land surface modelling. Hydrol. Earth Syst. Sci. 21, 1051–1062.

Graham, S.L., Laubach, J., Hunt, J.E., Mudge, P.L., Nuñez, J., Rogers, G.N.D., Buxton, R. P., Carrick, S., Whitehead, D., 2022. Irrigation and grazing management affect leaching losses and soil nitrogen balance of lucerne. Agric. Water Manag. 259, 107233.

Gupta, H.V., Kling, H., Yilmaz, K.K., Martinez, G.F., 2009. Decomposition of the mean squared error and NSE performance criteria: implications for improving hydrological modelling. J. Hydrol. 377 (1–2), 80–91. https://doi.org/10.1016/j.jhydrol.2009.08.003.

Hanson, B.R., Šimůnek, J., Hopmans, J.W., 2006. Evaluation of urea–ammonium–nitrate fertigation with drip irrigation using numerical modeling. Agric. Water Manag. 86, 102–113.

Hu, W., Tabley, F., Beare, M., Tregurtha, C., Gillespie, R., Qiu, W., Gosden, P., 2018. Short term dynamics of soil physical properties as affected by compaction and tillage in a silt loam soil. Vadose Zone J. 17 (180115) https://doi.org/10.2136/vzj2018.06.0115.

Inforsato, L., de Jong van Lier, Q.D.J., 2021. Polynomial functions to predict flux-based field capacity from soil hydraulic parameters. Geoderma 404, 115308. https://doi.org/10.1016/j.geoderma.2021.115308.

de Jong van Lier, Q., Wendroth, O., 2016. Reexamination of the field capacity concept in a Brazilian oxisol. Soil Sci. Soc. Am. J. 80, 264–274.

Kalfas, J.L., Xiao, X., Vanegas, D.X., Verma, S.B., Suyker, A.E., 2011. Modeling gross primary production of irrigated and rain-fed maize using MODIS imagery and CO_2 flux tower data. Agric. For. Meteorol. 151, 1514–1528.

Kelly, T.D., Foster, T., Schultz, D.M., 2023. Assessing the value of adapting irrigation strategies within the season. Agric. Water Manag. 275, 107986 https://doi.org/10.1016/j.agwat.2022.107986.

Ket, P., Oeurng, C., Degre, A., 2018. Estimating Soil water retention curve by inverse modelling from combination of in situ dynamic soil water content and soil potential data. Soil Syst. 2, 1–23. https://doi.org/10.3390/soilsystems2040055.

Klocke, N.L., Watts, D.G., Schneekloth, J.P., Davison, D.R., Todd, R.W., Parkhurst, A.M., 1999. Nitrate leaching in irrigated corn and soybean in a semi-arid climate. Trans. ASAE 42 (6), 1621–1630.

Kumar, H., Srivastava, P., Lamba, J., Diamantopoulos, E., Ortiz, B., Morata, G., Takhellambam, B., Bondesan, L., 2022. Site-specific irrigation scheduling using one-layer soil hydraulic properties and inverse modeling. Agric. Water Manag. 273, 107877 https://doi.org/10.1016/j.agwat.2022.107877.

Leij, F.J., Haverkamp, R., Fuentes, C., Zatarain, Z., Ross, P.J., 2005. Soil water retention: II. Derivation and application of shape index. Soil Sci. Soc. Am. J. 69, 1891–1901.

Lena, B.P., Bondesan, L., Pinheiro, E.A.R., Ortiz, B.V., Morata, G.T., Kumar, H., 2022. Determination of irrigation scheduling thresholds based on HYDRUS-1D simulations of field capacity for multilayered agronomic soils in Alabama, USA. Agric. Water Manag. 259, 107234 https://doi.org/10.1016/J.AGWAT.2021.107234.

Létourneau, G., Caron, J., Anderson, L., Cormier, J., 2015. Matric potential-based irrigation management of field-grown strawberry: effects on yield and water use efficiency. Agric. Water Manag. 161, 102–113. https://doi.org/10.1016/j.agwat.2015.07.005.

Meyer, P.D., Gee, G.W., 1999. Flux-based estimation of field capacity. J. Geotech. Geoenviron. Eng. 125, 595–599.

Minasny, B., McBratney, A., 2003. Integral energy as a measure of soil-water availability. Plant Soil 249, 253–262.

Mualem, Y., 1976. A new model for predicting the hydraulic conductivity of unsaturated porous media. Water Resour. Res. 12, 513–522.

Nachabe, M.H., 1998. Refining the definition of field capacity in the literature. J. Irrig. Drain. Eng. 124, 230–232.

Nasta, P., Gates, J.B., 2013. Plot-scale modeling of soil water dynamics and impacts of drought conditions beneath rainfed maize in Eastern Nebraska. Agric. Water Manag. 128, 120–130.

Nasta, P., Romano, N., 2016. Use of a flux-based field capacity criterion to identify effective hydraulic parameters of layered soil profiles subjected to synthetic drainage experiments. Water Resour. Res. 52. https://doi.org/10.1002/2015WR016979.

Nasta, P., Bonanomi, G., Šimůnek, J., Romano, N., 2021. Assessing the nitrate vulnerability of shallow aquifers under Mediterranean climate conditions. Agric. Water Manag. 258, 107208 https://doi.org/10.1016/j.agwat.2021.107208.

Ogata, G., Richards, L.A., 1957. Water content changes following irrigation of bare-field soil that is protected from evaporation. Soil Sci. Soc. Am. Proc. 21, 355–356.

Payero, J.O., Tarkalson, D.D., Irmak, S., Davison, D., Petersen, J.L., 2008. Effect of irrigation amounts applied with subsurface drip irrigation on corn evapotranspiration, yield, water use efficiency, and dry matter product in a semiarid climate. Agric. Water Manag. 95 (8), 895–908. https://doi.org/10.1016/j.agwat.2008.02.015.

Ramos, T.B., Šimůnek, J., Gonçalves, M.C., Martins, J.C., Prazeres, A., Pereira, L.S., 2012. Two-dimensional modeling of water and nitrogen fate from sweet sorghum irrigated with fresh and blended saline waters. Agric. Water Manag. 111, 87–104. https://doi.org/10.1016/j.agwat.2012.05.007.

Reynolds, W.D., 2018. An analytic description of field capacity and its application in crop production. Geoderma 326, 56–67.

Richards, L.A., 1931. Capillary conduction of liquids through porous medium. Physics 1, 318–333.

Ritchie, J.T., 1981. Soil water availability. Plant Soil 58, 327–338.

Romano, N., Santini, A., 2002. Water retention and storage: field. In: Dane, J.H., Topp, G. C. (Eds.), Methods of Soil Analysis, Part 4: Physical Methods. Soil Science Society of America, Madison, WI, pp. 721–738.

Romano, N., Brunone, B., Santini, A., 1998. Numerical analysis of one-dimensional unsaturated flow in layered soils. Adv. Water Resour. 21, 315–324.

Romano, N., Palladino, M., Chirico, G.B., 2011. Parameterization of a bucket model for soil-vegetation-atmosphere modeling under seasonal climatic regimes. Hydrol. Earth Syst. Sci. 15, 3877–3893.

Rudnick, D.R., Irmak, S., Ferguson, R.B., Shaver, T., Djaman, K., Slater, G., Bereuter, A., et al., 2016. Economic return versus crop water productivity of maize for various nitrogen rates under full irrigation, limited irrigation, and rainfed settings in South Central Nebraska. J. Irrig. Drain. Eng. 142 (6), 04016017. https://doi.org/10.1061/(ASCE)IR.1943-4774.0001023.

Rudnick, D.R., Irmak, S., West, C., Chávez, J.L., Kisekka, I., Marek, T.H., et al., 2019. Deficit irrigation management of maize in the High Plains aquifer region: a review. J. Am. Water Resour. Assoc. 55 (1), 38–55. https://doi.org/10.1111/1752-1688.12723.

Samani, B., Samani, S., Yang, H., Yu, H., 2020. Uncertainty analysis and visualization for nitrogen leaching with the maize-N model. In: Proceedings of the IEEE International Conference on Big Data (Big Data), Atlanta, GA, USA, 2020, pp. 3295–3303. ⟨DOI: 10.1109/BigData50022.2020.9378105⟩.

Sao, D., Saito, H., Kato, T., Šimůnek, J., 2021. Numerical analysis of soil water dynamics during spinach cultivation in soil column with an artificial capillary barrier under different irrigation managements. Water 13 (2176), 18. https://doi.org/10.3390/w13162176.

Scanlon, B.R., Faunt, C.C., Longuevergne, L., Reedy, R.C., Alley, W.M., McGuire, V.L., McMahon, P.B., 2012. Groundwater depletion and sustainability of irrigation in the US High Plains and Central Valley. Proc. Natl. Acad. Sci. USA 109 (24), 9320–9325. https://doi.org/10.1073/pnas.1200311109.

Schlüter, S., Großmann, C., Diel, J., Wu, G.-M., Tischer, S., Deubel, A., Rücknagel, J., 2018. Long-term effects of conventional and reduced tillage on soil structure, soil ecological and soil hydraulic properties. Geoderma 332, 10–19. https://doi.org/10.1016/j.geoderma.2018.07.001.

Sharma, V., Irmak, S., 2020. Economic comparisons of variable rate irrigation and fertigation with fixed (uniform) rate irrigation and fertigation and pre-plant fertilizer management for maize in three soils. Agric. Water Manag. 240, 106307 https://doi.org/10.1016/j.agwat.2020.106307.

Šimůnek, J., Šejna, M., van Genuchten, M.T., 2016. Recent developments and applications of the HYDRUS computer software packages. Vadose Zone J. 15 (7), 1–25. https://doi.org/10.2136/vzj2016.04.0033.

Šimůnek, J., van Genuchten, M.Th., Sejna, M., 2006. The HYDRUS Software Package for Simulating the Two- and Three-Dimensional Movement of Water, Heat, and Multiple Solutes in Variably-Saturated Media, Technical Manual, Version 1.0.

Soil Science Society of America, 2008. Glossary of Soil Science Terms. SSSA, Madison, WI, ISBN 978-0-89118-851-3, 7, p. 92.

Soil Survey Division Staff, 2017. Soil survey manual fourth. In: Ditzler, C., Scheffe, K.K., Monger, H.C. (Eds.), USDA Handbook 18. USDA-Natural Resources Conservation Service. Government Printing Office, Washington, D.C.

Srinivasan, M.S., Measures, R., Fear, A., Elley, G., 2022. Making the invisible visible: co-learning guided development of an operational tool for irrigation management. Agric. Water Manag. 264, 107492 https://doi.org/10.1016/j.agwat.2022.107492.

Suyker, A., Verma, S., Burba, G., Arkebauer, T., Walters, D., Hubbard, K., 2004. Growing season carbon dioxide exchange in irrigated and rainfed maize. Agric. For. Meteorol. 124, 1–13.

Suyker, A.E., Verma, S.B., 2008. Interannual water vapor and energy exchange in an irrigated maize-based agroecosystem. Agric. For. Meteorol. 148, 417–427.

Suyker, A.E., Verma, S.B., 2009. Evapotranspiration of irrigated and rainfed maize–soybean cropping systems. Agric. For. Meteorol. 149, 443–452.

Talukder, R., Plaza-Bonilla, D., Cantero-Martínez, C., et al., 2022. Spatio-temporal variation of surface soil hydraulic properties under different tillage and maize-based crop sequences in a Mediterranean area. Plant Soil. https://doi.org/10.1007/s11104-022-05758-x.

Taylor, S.A., Ashcroft, G.L., 1972. Physical Edaphology: The Physics of Irrigated and Nonirrigated Soils. W.H. Freeman, San Francisco.

Thomasson, A.J., 1995. Assessment of soil water reserves available for plants (SWAP): a review. In: King, D., Jones, R.J.A., Thomasson, A.J. (Eds.), European Land Information Systems for Agro-environmental Monitoring. EUR 16232 EN, Office for Official Publications of the European Communities, Luxembourg, 115130.

Torres, L.C., Keller, T., de Lima, R.P., Tormena, C.A., de Lima, H.V., Giarola, N.F.B., 2021. Impacts of soil type and crop species on permanent wilting of plants. Geoderma 384, 114798. https://doi.org/10.1016/j.geoderma.2020.114798.

Turek, M.E., van Lier, Q., de, J., Armindo, R.A., 2020. Estimation and mapping of field capacity in Brazilian soils. Geoderma 376, 114557.

Turek, M.E., de Jong van Lier, Q.D.J., Armindo, R.A., 2022. Parameterizing field capacity as the upper limit of available water in bucket-type hydrological models. Comput. Electron. Agric. 194, 106801.

Turkeltaub, T., Ascott, M.J., Gooddy, D.C., Jia, X., Shao, M.-A., Binley, A., 2020. Prediction of regional-scale groundwater recharge and nitrate storage in the vadose zone: a comparison between a global model and a regional model. Hydrol. Proc. 34, 3347–3357. https://doi.org/10.1002/hyp.13834.

Twarakavi, N.K.C., Sakai, M., Šimůnek, J., 2009. An objective analysis of the dynamic nature of field capacity. Water Resour. Res. 45, 1–9.

van Genuchten, M.Th, 1980. A closed form equation for predicting the hydraulic conductivity of unsaturated soils. Soil Sci. Soc. Am. J. 44, 892–898.

Veihmeyer, F.J., Hendrickson, A.H., 1949. Methods of measuring field capacity and wilting percentages of soils. Soil Sci. 68, 75–94.

Verma, S.B., Dobermann, A., Cassman, K.G., Walters, D.T., Knops, J.M., Arkebauer, T.J., Suyker, A.E., Burba, G.G., Amos, B., Yang, H., Ginting, D., 2005. Annual carbon dioxide exchange in irrigated and rainfed maize-based agroecosystems. Agr. For. Meteorol. 131, 77–96.

Vogeler, I., Thomas, S., van der Weerden, T., 2019. Effect of irrigation management on pasture yield and nitrogen losses. Agric. Water Manag. 216, 60–69. https://doi.org/10.1016/j.agwat.2019.01.022.

Weitzman, J.N., Brooks, J.R., Compton, J.E., Faulkner, B.R., Mayer, P.M., Peachey, R.E., Rugh, W.D., Coulombe, R.A., Hatteberg, B., Hutchins, S.R., 2022. Deep soil nitrogen storage slows nitrate leaching through the vadose zone. Agric. Ecosyst. Environ. 332, 107949.

Wesseling, J.G., Elbers, J.A., Kabat, P., Van den Broek, B.J., 1991. SWATRE: Instructions for Input. Internal Note, Winand Staring Centre, Wageningen, the Netherlands.

Wiecheteck, L.H., Giarola, N.F.B., de Lima, R.P., Tormena, C.A., Torres, L.C., de Paula, A. L., 2020. Comparing the classical permanent wilting point concept of soil (−15,000 hPa) to biological wilting of wheat and barley plants under contrasting soil textures. Agric. Water Manag. 230, 105965 https://doi.org/10.1016/j.agwat.2019.105965.

Wilcox, J.C., 1959. Rate of soil drainage following an irrigation. I. Nature of soil drainage curves. Can. J. Soil Sci. 19, 107–119.

Wöhling, T., Vrugt, J.A., 2011. Multiresponse multilayer vadose zone model calibration using Markov chain Monte Carlo simulation and field water retention data. Water Resour. Res. 47, W04510. https://doi.org/10.1029/2010WR009265.

Wollschläger, U., Pfaff, T., Roth, K., 2009. Field-scale apparent hydraulic parameterisation obtained from TDR time series and inverse modelling. Hydrol. Earth Syst. Sci. 13, 1953–1966.

Zhang, J., Guan, K., Peng, B., Jiang, C., Zhou, W., Yang, Y., Pan, M., Franz, T.E., Heeren, D.M., Rudnick, D.R., 2021a. Challenges and opportunities in precision irrigation decision-support systems for center pivots. Environ. Res. Lett. 16 (5), 53003.

Zhang, J., Guan, K., Peng, B., Pan, M., Zhou, W., Jiang, C., Kimm, H., Franz, T.E., Grant, R.F., Yang, Y., 2021b. Sustainable irrigation based on co-regulation of soil water supply and atmospheric evaporative demand. Nat. Commun. 12 (1), 1–10.

Zotarelli, L., Dukes, M.D., Morgan, K.T., 2019. Interpretation of Soil Moisture Content to Determine Soil Field Apacity and Avoid Over-irrigating Sandy Soils Using Soil Moisture Sensors. Agricultural and Biological Engineering Department, UF/IFAS Extension, AE460, pp. 1–4.